Journal of Paleolimnology (2006) 35:417–439
DOI 10.1007/s10933-005-1996-1

Is there a paleolimnological explanation for 'walking on water' in the Sea of Galilee?

Doron Nof[1,2,*], Ian McKeague[3,4] and Nathan Paldor[5]
*[1]Department of Oceanography, Florida State University, Tauahassee, FL 32303, U.S.A.; [2]Geophysical Fluid Dynamics Institute, Florida State University, Tauahassee, FL 32303, U.S.A.; [3]Department of Statistics, Florida State University; [4]presently at Department of Biostatistics, Columbia University; [5]Department of Atmospheric Science, The Hebrew University of Jerusalem; *Author for correspondence (e-mail: nof@ocean.fsu.edu)*

Received 13 April 2005; accepted in revised form 1 August 2005

Key words: 'Walking on water', Air–lake interaction, Convection, Lake freezing, Salty springs

Abstract

Lake Kinneret (the Sea of Galilee) is a small freshwater lake (148 km^2 and a mean depth of 20 m) situated in northern Israel. Throughout recent history there have been no known records of a total ice formation on its top. Furthermore, given that convection requires an initial cooling of the entire lake down to 4 °C, it is difficult to imagine how such a low-latitude lake, presently subject to two-digit temperatures during the winter, could ever freeze. Lake Kinneret is, however, unique in the sense that there are dense (warm and salty) springs along its western shore. The dynamics of the regions adjacent to these springs are investigated using a one-dimensional nonlinear analytical ice model, a paleoceanographic record of the sea surface temperature of the Mediterranean Sea, and a statistical model. We show that, because the water directly above the plume created by the salty springs does not convect when it is cooled down to 4 °C, freezing of the region directly above the salty springs was possible during periods when the climate in the region was somewhat cooler than it is today. We refer to this localized freezing situation as 'springs ice'.

The analytical ice-model involves a slowly varying approach where the ice is part of a thin fresh and cold layer floating on top of the salty and warm spring water below. During the ice formation process, the ice is cooled by the atmosphere above and warmed by the spring water below. The plumes created by the springs have a length scale of 30 m, and it is argued that, during the Younger Dryas when the air temperature in the region was probably 7 °C or more cooler than today, 'springs ice' (thick enough to support human weight) was formed once every 27 years or less. During the cold events 1500 and 2500 years ago (when the atmospheric temperature was 3 °C or more lower than today) springs ice occurred about once in 160 years or less. Since the duration of these cold events is of the same order as the springs ice recurrence time, there is a substantial chance that at least one springs ice occurred during these cooler periods. With today's climate, the likelihood of a springs ice is virtually zero (i.e., once in more than 10,000 years).

One set of those springs associated with the freezing is situated in Tabgha, an area where many archeological features associated with Jesus Christ have been found. On this basis, it is proposed that the unusual local freezing process might have provided an origin to the story that Christ walked on water. Since the springs ice is relatively small, a person standing or walking on it may appear to an observer situated some distance away to be 'walking on water'. This is particularly true if it rained after the ice was formed (because rain smoothes out the ice's surface). Whether this happened or not is an issue for religion scholars, archeologists, anthropologists, and believers to decide on. As natural

scientists, we merely point out that unique freezing processes probably happened in that region several times during the last 12,000 years.

Nomenclature
Symbols:
T – temperature;
C_{pa}, C_{pw} – heat capacity of air, water;
C_D – non-dimensional drag coefficient;
D – ice thickness;
u – mean plume speed;
U – wind speed;
L – plume width;
g – gravity;
g' – "reduced gravity,"$(g\Delta\rho/\rho)$;
k – thermal conductivity;
S – salinity;
H – upper layer thickness;
$\hat{H}$ – plume thickness;
Q – springs volume flux;
a – diffusivity coefficient;
α, β – constants defined by (4.5);
δ – plume veering angle;
ρ_a, ρ_w – density of air, water;
φ – heat flux;
λ_i – ice heat of fusion;
μ – bottom slope;
μ_0 – off-shore bottom slope

Introduction

This article contains two quite different components. The first is a rigorous theoretical analysis of the conditions under which local freezing could have happen along the shores of Lake Kinneret during the last 12,000 years. This component is done using conventional scientific methods. The second component contains the plausible hypothesis that the story of Christ 'walking on water' originated from this unusual freezing. By its very nature, this second component is less rigorous than the first one. Nevertheless, the two components are intertwined and are presented together because the first component was developed in order to examine the second. While most reconstructions of lakes histories are based on cores and sediments analysis, the reconstruction here is based primarily on models.

The reader is warned in advance that it may be quite difficult to follow the analysis because it involves five very different areas of physical oceanography and limnology: paleoceanogarphic analysis of the Mediterranean sea surface temperature with both simple and complicated climate models, an analysis of the springs characteristics during the cold events, plume dynamics, ice dynamics, and a statistical analysis. Furthermore, each of these five sections is, by itself, fairly involved.

The lake and the springs

Lake Kinneret is situated 45 km east of the Mediterranean eastern shoreline at approximately 32 °N. It is roughly 8 × 18 km with a maximum depth of 44 m (Figure 1). It is stratified during the summer and well-mixed in the winter. Although it is a fresh-water lake, its salinity is relatively high [approximately 0.5 practical salinity units (PSU); the reader who is interested in these common salinity units is referred to any introductory book on physical oceanography] because of both underwater and above-water saltwater springs. The origin of the springs is still under debate. Their location (on the western edge of the lake) suggests that they could perhaps be associated with a flow from the Mediterranean Sea that stands about 200 m higher, providing a gradient of about 5 m per kilometer. Another possibility is that the springs are a remnant of water that percolated into the aquifer during the period that salty Lake Lisan (a paleo salty lake which incorporated both the Dead Sea and Lake Kinneret, and stood approximately 20 m higher than the current lake level) was still present. When the salty lake water level subsided, the percolated salty water started pouring back into the lake (Hurwitz et al. 2000).

Because of agricultural and urban development, the present lake is nothing like it was before significant human impacts. During the first half of the 20th century, Lake Hula, a wetland (approxi-

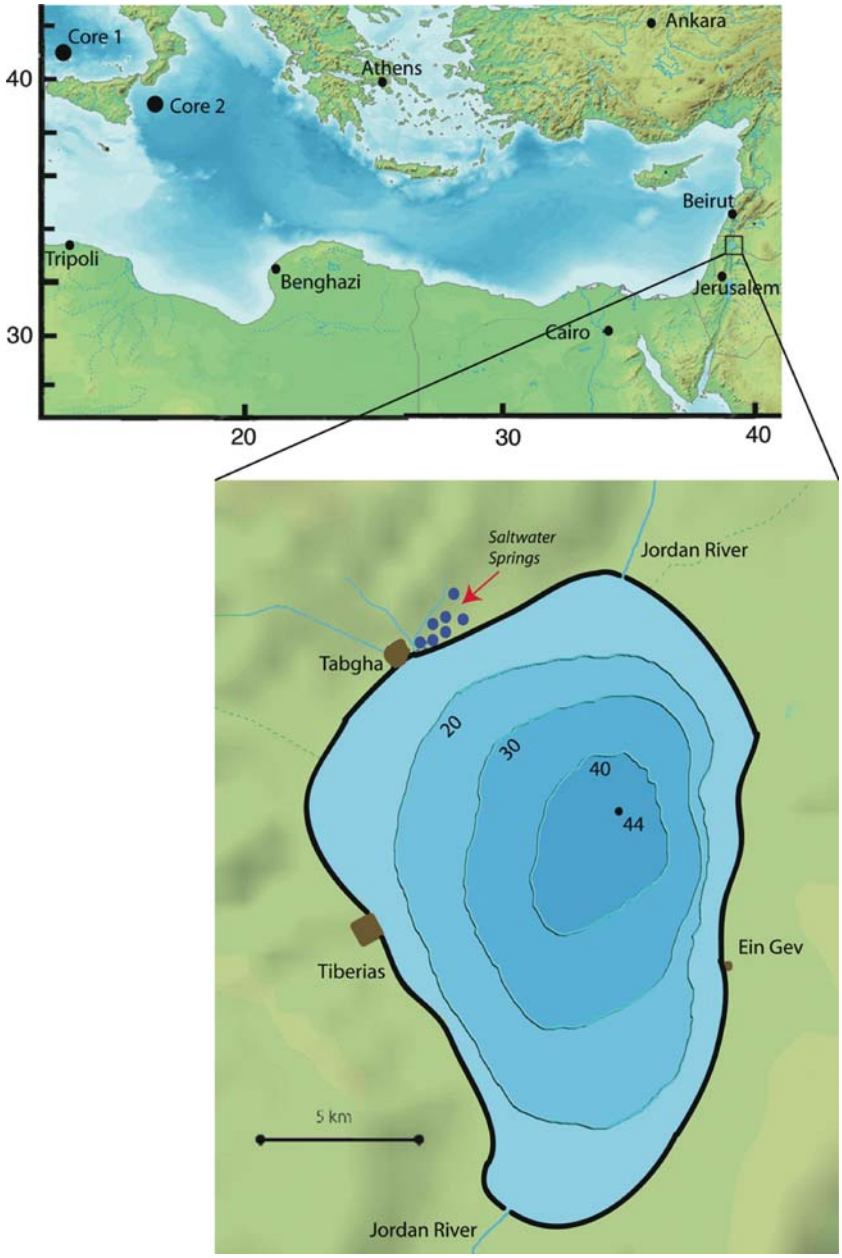

Figure 1. A map of Lake Kinneret with the position of the Tabgha warm and salty springs. The locations of the Central Mediterranean cores on which Figure 2 is based are also shown. Depth contours is given in meters.

mately 5 × 10 km) situated north of Lake Kinneret, was converted into agricultural fields. The Jordan River, which empties into the northern part of Lake Kinneret, used to flow through this wetland, which probably warmed its cold spring-fed water. During the 1960s, the salty and warm springs at Tabgha (loose Arabic pronunciation of *Heptapegon* meaning 'seven springs' in Latin), and other springs located nearby, were diverted into the downstream part of the Jordan River (i.e., the part of the river which is south of Lake Kinneret). The lake is a major source of fresh water for the region and it was hoped that this diversion would lower its relatively high salinity (0.5 PSU). It did, but, due to the submerged springs and other processes, the reduction was fairly limited.

During the summer, the winds over Lake Kinneret are primarily due to: (i) sea breezes associated with the Mediterranean Sea, (ii) lake breeze, and (iii) katabatic winds associated with the surrounding mountains (see, e.g., Antenucci and Imberger 2003 and the references given therein). During the winter, on the other hand, the winds are primarily due to winter storms over the Mediterranean Sea. As a result, the lake area is subject to stronger winds during the winter (when the low pressure anomaly just reaches the region) but these stronger winds occur less frequently than the strong summer winds. Furthermore, these winter winds usually die-off after the outer edges of the low pass by.

Humans have been active along the lake for many years and, recently, archeological excavations have unearthed 23,000-year-old mats (Nadel et al. 2004). Evidently, Jesus Christ spent a significant amount of time in Tabgha (see, e.g., Pixner 1985) and the 'walking on water' account might have originated there. [Matthew 14:25: And in the fourth watch of the night Jesus went unto them, walking on the sea. 14:26 And when the disciples saw him walking on the sea, they were troubled, saying, It is a spirit; and they cried out for fear. 14:27 But straightway Jesus spake unto them, saying, Be of good cheer; it is I; be not afraid. 14:28 And Peter answered him and said, Lord, if it be thou, bid me come unto thee on the water.]

Our analysis

We shall begin our analysis by presenting paleoceanographic temperature data from the central Mediterranean Sea showing cooling events during the last 13,000 years (Section 2). These cores were taken 2000 km away from Lake Kinneret but they represent the closest paleoclimate records that exist. We shall show that, during the above period, there have been several cooling events where the sea surface temperature (SST) was 1–5 °C cooler than it is today. We shall relate these SST anomalies to the atmospheric anomalies above using both a novel simple model involving heat exchange and Ekman dynamics and the results of recent general climate models (GCMs) which include much more variables than our model does. The simple model shows that the *maximum* ratio of the SST anomalies to the atmospheric temperature anomalies above is the air/water heat capacities ratio, which is roughly 1:4. This implies that, since it is easier to cool the atmosphere than it is to cool the ocean, the atmospheric anomalies can be as high as four times the oceanic anomalies. It turns out that this is probably true for high latitudes but, for low latitudes, GCMs runs suggest a smaller ratio of atmospheric to oceanic anomalies, about 1.5–2.0. We shall do our calculations for both the low and high values so that we will cover the entire possible range.

We shall then present the analysis of stalactites in the Soreq cave in southern Israel (approximately 35 ° E, 31 ° N) and show that these cooling events were associated with an increased aridity. We shall then proceed and examine the scales of the plumes created by the salt water springs (Section 3). It will be demonstrated that the plume moves primarily along the coast gradually veering to the left of the isobaths (looking downstream). Using the decreased aridity record, we shall also estimate the salinity of the springs during the cold events.

We shall continue with an examination of the conditions under which freezing above the plumes (resulting from the springs) could take place. In this context, we shall note that a 'regular' freezing of a fresh water lake with dimensions similar to Lake Kinneret would require *a few or several months* of near- or below-freezing temperatures because the density of fresh water (and even brackish water) reaches a maximum around 4 °C. Consequently, convection occurs around this temperature implying that the entire lake needs to be first cooled down to 4 °C. Any further cooling produces lighter water which stays on top and finally freeze. The freezing of such 'regular' lakes require relatively large amounts of cooling because, as mentioned, much cooling needs to be done *before* cooling processes can go directly to the formation of ice on top. Lake Mendota in central Wisconsin (approximately 89 ° W, 43 ° N) is about 25% the size of Lake Kinneret and provides a good example of such a lake (see, e.g., Dutton and Bryson 1962). Rough estimates suggest that, even during the Younger Dryas and the last glacial maximum (LGM) when the estimated atmospheric temperature reduction was relatively

high, a complete cooling of the entire lake to 4 °C is extremely unlikely. [Without a more detailed knowledge of the evaporation rate and other variables during the Younger Dryas and the last glacial maximum (LGM), it is impossible to unequivocally say whether winter freezing occurred or not.]

For the warmer Holocene, the possibility of a period of a few or several months of near-freezing temperatures is even less likely. Consequently, we rule this conventional general freeze out for the relatively low latitude of Lake Kinneret. Using one-dimesional analytical models, we shall demonstrate, however, that local 'springs ice' (i.e., freezing and ice formation in a confined region directly above the plumes created by the salty springs) requires merely a few *days* of below-freezing temperatures. This is because the salty springs water creates a strong salt-induced stratification (above the plume) that inhibits convection. Consequently, the cooling process goes immediately to ice formation on top rather than toward convection and a total cooling of the entire lake to 4 °C. Note, however, that the required cold spell of a few days must be relatively calm, with wind speeds of less than, say, 6 m/s. Otherwise, the wind would mix the plume into the fresh water above, destroying the stratification and preventing a no-convection cooling process. Such calm periods are very common around the lake.

After presenting the plumes' details in Section 3, we describe the ice-model in Section 4. In that section, we employ the slowly varying approach and derive a single first-order nonlinear differential equation incorporating heat exchange with both the cold atmosphere above and the warm saline water below. An exact solution (which is not entirely new) is found and its analysis is given in the same section (4) where we show how long it would take to form an ice layer of 10 cm thickness on top of the plumes. (Such a layer is certainly sufficient to accommodate the weight of humans on top of it: on the basis of Red Cross recommendations, many municipalities require 15 cm of ice for safe ice skating.) Note that the use of one-dimensional models to examine freezing processes in lakes is adequate as a first approximation because high-resolution three-dimensional numerical models typically display very similar results (Omstedt 1999).

We then proceed, using a statistical model, to calculate the likelihood that such a period of below-freezing temperatures would take place (Section 5). We do this for various mean temperature reductions corresponding to the known cooling events that took place during the last 13,000 years. This is followed by an analysis of the conditions under which there will be a few consecutive days of no wind stronger than 6 m/s. The results are summarized in Section 6.

The paleoceanographic temperature record

Unfortunately, there are no direct (or indirect) paleoclimatic records from the Lake Kinneret region. What we can do is use paleo-records of sea surface temperature (SST) from regions in the Mediterranean some distance away from the lake (approximately 2000 km) because this distance is not any greater than the typical weather system scale in that part of the world. This approach is justified because the winds in the region are usually from the west so that the air above the lake usually originates in the atmospheric boundary layer above the Mediterranean Sea. In other words, it is reasonable to take the Mediterranean SST as indicative of the Middle East climate – some claim that even regions in the Atlantic (and the North Atlantic Oscillation) correlate with temperatures in the Middle East (e.g., Eshel and Farrell 2000, Eshel et al. 2000, Cullen et al. 2002).

Sea surface temperature

Figure 2 shows the sea surface temperature (SST) record for the past 16,000 years as determined from two cores, one taken near the northwest corner of Sicily (adapted from Cacho et al. 2001) and the other in the Ionian Sea (adapted from Emeis et al. 2000). The location of the cores is shown in Figure 1. The first core was chosen because, of all the cores presented by Cacho et al. (2003), it is the most representative of the water entering the eastern Mediterranean. As mentioned, since the synoptic atmospheric scale is of the order of 1000 km, it is this SST which determines the air temperature above the lake.

The Cacho's core starts around 1000 years ago and we related it to the present-day climate with

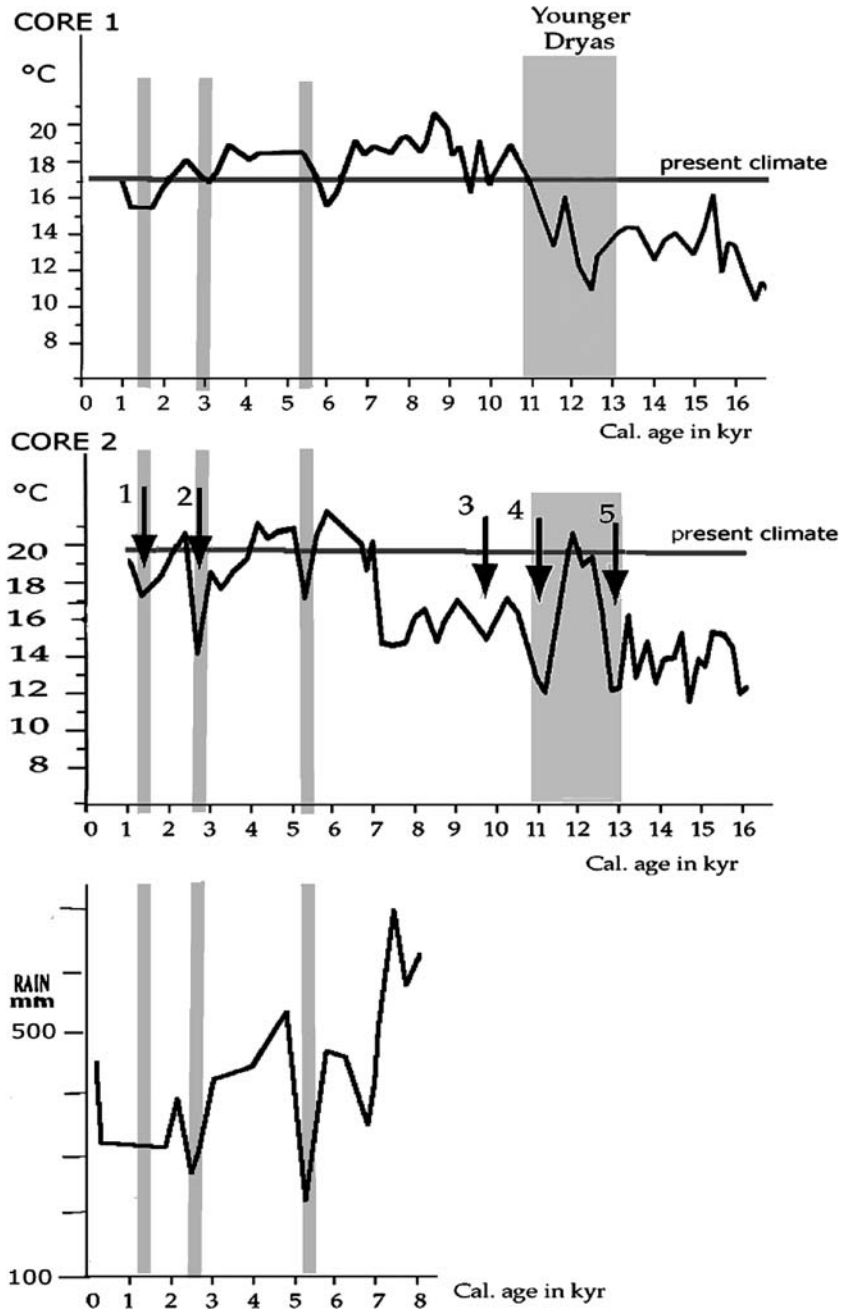

Figure 2. Upper two panels: The sea-surface temperature (SST) record during the last 16,000 years, determined from two cores, one situated slightly to the northeast of the Strait of Messina (see Fig. 1), and the other situated in the Ionian Sea (adapted from Cacho et al. 2001, and Emeis et al. 2000). Note that, both records reflect cold events when the temperature dropped significantly below the present day temperature (horizontal line). For convenience, they are only marked in the middle panel (see text). Lower panel: The rainfall record during the last 8000 years as determined from stalactites in the Soreq cave in southern Israel (adapted from Bar-Matthews et al. 2003). Note the correlation between the cold events and an increased aridity (vertical grey lines at 1500, 2500 and 5300 years ago).

the aid of Reale and Dirmeyer (2000) analysis. On the basis of archaeological and historical data, they argue that 2000 years ago the climate was as warm as it is today [see (their) page 165]. Hence, we take the Cacho's temperature 2000 years ago to be today's temperature (see the horizontal gray

Table 1. Significant cooling events during the last 13,000 years.

Event	Years BP	Temp. reduction, Core 1 (°C)	Temp. reduction, Core 2 (°C)	Approx. mean reduction (°C)
1	1500	−2	−2	−2
2	2500	+1	−5	−2
3	9800	0	−4	−2
4	11,000	−1	−8	−5
5	12,800	−3	−7	−5

line in the upper panel of Figure 2). For consistency, we did the same with Emeis' record (see the horizontal line in the middle panel of Figure 2). Since Emeis' record extended to the present day, this consistency requirement implied that the first few hundred years of Emeis' record had to be disregarded. This period corresponds to the first few centimeters of their core and, hence, may not be representative of the actual situation because of disturbances that might have been introduced either by the coring device itself or by recent strong flows along the bottom that altered the upper sediment (via scouring or depositing).

Table 1 shows the cooling events that the two cores display. Some events occur in both cores at the same time and others do not. We chose five events (1500, 2500, 9800, 11,000 and 12,800 years ago) that are shown with arrows near the record of the second core (Figure 2). We averaged the temperatures at these particular times even though a cooling event in one record does not necessarily correspond to a cooling event in the other record. The mean cooling of the first three events (1500, 2500 and 9800 years ago) turns out to be roughly 2 °C and the last two (11,000 and 12,800 years ago) correspond to a mean cooling of about 5 °C. Note that other choices could have been made. For example, we chose not to consider the cooling event 5300 years ago (not numbered in the middle panel) but one could certainly consider it as well. We chose not to, merely because it is considerably smaller than the others (i.e., it corresponds to a mean SST reduction of about 1 °C). It will become clear later that this relatively small cooling implies that the recurrence time for a springs ice is more than a 1000 years – longer than the cooling event itself.

It is important to realize that the above SST coolings during the Younger Dryas and earlier are consistent with ground water cooling in Oman [situated about 2000 km to the southeast of the Sea of Galilee (Weyhenmeyer et al. 2000)], with SST cooling in Barbados (Guilderson et al. 1994) and Venezuela (Lea et al. 2003), and with ground water estimates in Brazil (Stute et al. 1995). Although there have been some questions regarding the ground water temperature estimates, the above suggest that the Mediterranean cores are representative of the anomalies in the region surrounding the lake. (As mentioned, it is unfortunate that there are no cores closer to the lake – the only ones that are available do not extent more than 800 years before present.)

Figure 2 also shows the rainfall during the last 8000 years as determined from stalactites in the Soreq cave in southern Israel (adapted from Bar-Matthews et al. 2003). We note that, from the beginning of the Holocene to the present day, there has been a gradual decline in rainfall, in agreement with other studies. There are four events of reduced rainfall, three of which are clearly correlated with cooling events shown by the Ionian Sea core (see the vertical gray lines and the record of core 2 in Figure 2). This is also in agreement with other studies which showed that cooling events are associated with an increased aridity (e.g., De Rijk et al. 1997; Bartov et al. 2003). Bryson and Bryson (1998) also show a significantly decreased Nile fresh water flux during roughly the same period of increased aridity.

Interestingly, Bar-Matthews et al. (2003) compare their rainfall data to the SST reconstruction from a core taken south of Cyprus that shows an inverse correlation with the cooling events, i.e., a decreased rainfall is associated with warming rather than cooling [see (their) Fig.13A]. We believe that this is because this particular core is heavily influenced by the Nile which empties into the Mediterranean Sea a few hundred kilometers to the south. (Note that, before the construction of the Aswan High Dam, the discharge of the Nile River was much greater than it is today, about 1000 m^3/s.) Since river water is typically several degrees cooler than the ocean (because the ocean is usually warmer than the atmosphere), a reduced rainfall (and a resulting reduced river discharge) implies less cooling which, in the core record, is represented by an apparent warming. (Note that, even though the river water is cooler than the Mediterranean Sea, it is still buoyant because it is fresh.) Hence, the Bar-Matthews et al. (2003)

comparison is not really a comparison of rainfall to an independent Mediterranean SST but rather a comparison of rainfall to an SST which, by itself, is influenced by the rainfall.

Relation of the SST to the atmospheric temperature

We shall now relate the SST anomalies to the atmospheric anomalies above. Before doing so, it is appropriate to point out that the only place where both oceanic anomalies and atmospheric anomalies have been observed at the same time and the same location is the northern North Atlantic. Here, oceanographic proxy data gave the SST anomalies (for the last 100,000 years) whereas air bubbles trapped in the ice sheets over Greenland gave the corresponding atmospheric anomalies [see e.g., Bard (2002), the top two panels of (his) Figure 2]. For this case, the ratio of atmospheric temperature anomalies to SST anomalies is fairly high, approximately 3.5. Recent climate models runs suggest, on the other hand, that at least in low latitudes, this ratio is perhaps as small as 1.5 or 2.0 (e.g., Pinot et al. 1999; Shin et al. 2003). In what follows we shall use a simple dynamical model to show that the above ratio is, at the most, 4.0. We shall later perform our final calculations for both a ratio of 1.5 and a ratio of 4.0 so that we shall cover the entire possible range of anomalies.

We shall now present our simple novel argument suggesting that, during cold events, the *maximum* temperature reduction in the atmosphere is related to the oceanic reduction via the ratio of the air/water heat capacities. Consider the situation shown in Figure 3a, b. A one-dimensional box is oriented along the atmosphere geostrophic flow (Figure 3a). The mean Ekman flow in both the ocean and atmosphere are oriented at 45 ° and 135 ° relative to the box axis. Both have components perpendicular to the geostrophic flow (and the box axis) and these perpendicular components are denoted by Q_o and Q_a. As Figure 3a illustrates, they are equal to the Ekman fluxes divided by $\sqrt{2}$. Note that none of this information is new, all of it can be found in a variety of textbooks. It is listed here merely to illustrate how our box is oriented.

The oceanic volume flux Q_w enters the box where it cools from T_{wi} to T_{wo}. (The subscripts 'i' and 'o' denote 'in' and 'out.') The heat is released to the atmosphere (which has a volume flux Q_a) and, as a result, the atmosphere warms from T_{ai} to T_{ao}. This heat exchange between the ocean and the atmosphere can be written as,

$$\rho_w C_{pw} Q_w (T_{wi} - T_{wo}) = \rho_a C_{pa} Q_a (T_{ao} - T_{ai}), \quad (1)$$

where the subscripts 'w' and 'a' denote water and air, and C_{pa} and C_{pw} are the heat capacities. (For convenience, all variables are defined in both the text and the Nomenclature.) Note that this equation is simply a heat flux equation for a box and that, in the regions to the right and left of the box (Figure 3b), the ocean is insulated from the atmosphere. Also, it is assumed here that there is no heat exchange between the box and the fluid above or below.

Recalling that the atmospheric and oceanic Ekman mass fluxes are the same, we immediately get the relationship,

$$\rho_w Q_w = \rho_a Q_a. \quad (2)$$

Substitution of (2) into (1) gives,

$$T_{wi} - T_{wo} = \frac{C_{\rho a}}{C_{\rho w}} (T_{ao} - T_{ai}), \quad (3)$$

showing that the mean reduction in the oceanic temperature is related to the mean increase of the atmospheric temperature through the ratio of the air/water heat capacities (approximately 1:4). In a way, this is not very surprising – it is much easier to cool the air than it is to cool the water so that any local climatic anomaly is expected to be more pronounced in the air than in the water below.

Suppose further that, through some process whose details are not important for the present discussion, the incoming water temperature has been reduced so that the difference between the incoming and outgoing ocean water ($T_{wi} - T_{wo}$) has been temporarily reduced by, say, ΔT_w. (The reader who would like to envision a corresponding physical situation can think of the incoming water as, say, Atlantic water entering the Mediterranean through the Straits of Gibraltar.) Such a reduction would, in general, imply a change in both the ingoing and outgoing water temperatures but, to obtain the *maximum* heat exchange between the ocean and the air, we assume that it involves merely the lowering of the *incoming* ocean water temperature T_{wi} (i.e., we shall leave the outgoing water temperature T_{wo} unaltered). In reality, there will be some reduction of the outgoing oceanic water too

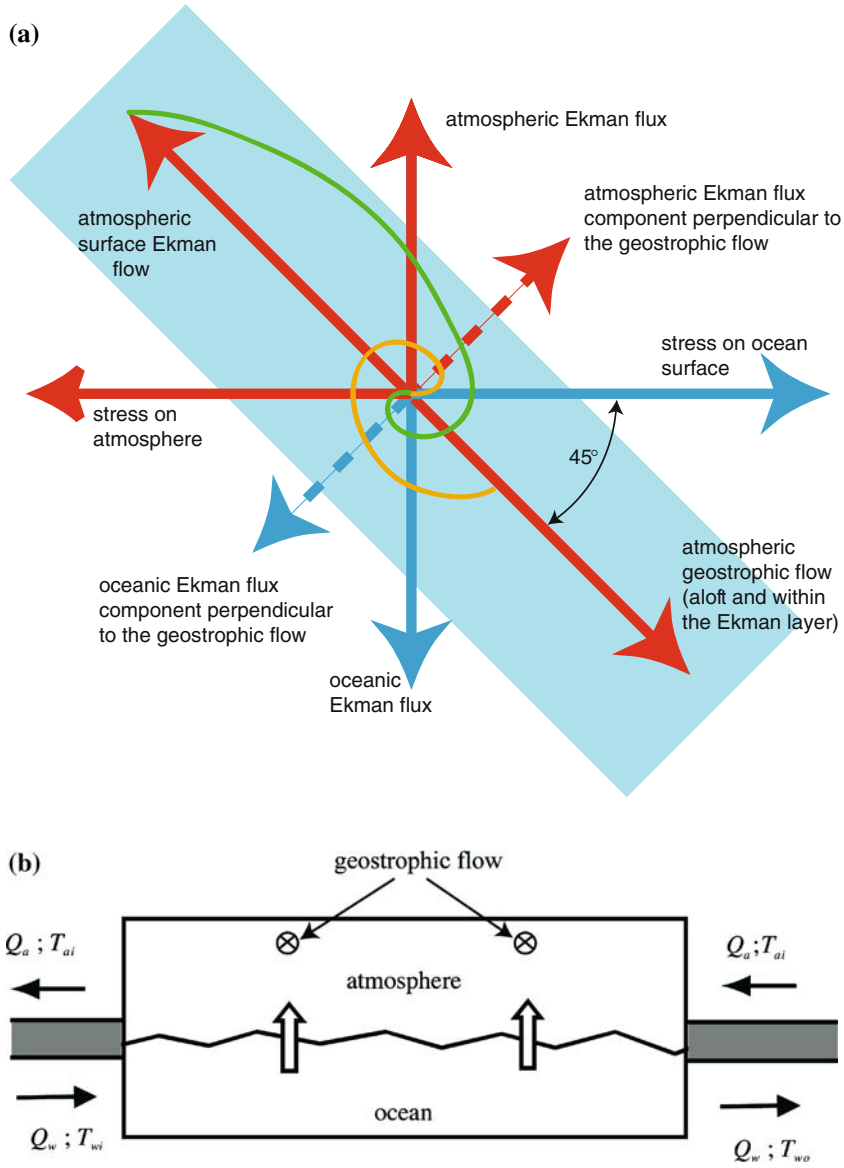

Figure 3. ((a) The orientation of the various fluxes in the ocean (blue lines) and atmosphere (red lines). The oceanic Ekman flux is oriented at 90 ° to the right of the stress exerted on the ocean by the atmosphere whereas the atmospheric Ekman flux is 90 ° to the left of that stress. The atmospheric geostrophic flow above and within the atmospheric Ekman layer is directed at 45 ° to the right of the stress exerted on the ocean by the atmosphere so that, at the surface, it exactly cancels the surface atmospheric Ekman flow which is directed at 135 ° to the left of the stress on the ocean surface. (This implies that, as should be the case, the sum of the two is zero at the surface.) The yellow and green spirals indicate the Ekman flow in the ocean and atmosphere (respectively). None of the information shown here is new. It is displayed merely to illustrate how the box shown in Fig. 3b is oriented (blue shading). (b) Schematic diagram of the simplified ocean–atmosphere heat exchange process. An oceanic volume flux Q_w (with an incoming temperature T_{wi} and an outgoing temperature T_{wo}) enters a one-dimensional box where it cools and releases its heat to the atmosphere (thick vertical arrows). The atmospheric volume flux Q_{a} has an incoming temperature T_{ai} and an outgoing temperature T_{ao}. The ocean is insulated from the atmosphere in regions to the right and left of the box. Both the oceanic and atmospheric fluxes represent the fraction of the Ekman flux which is perpendicular to the atmospheric geostrophic flow. (These amounts equal the total Ekman flux divided by $\sqrt{2}$.) The box is oriented along the atmospheric geostrophic flow (directed into the page).

so that only a fraction of the oceanic temperature anomaly will be transmitted to the atmosphere. However, since we are merely interested here in the *maximum* ocean–atmosphere exchange, we take this reduction of the outgoing water temperature to be zero so that the entire oceanic anomaly is communicated to the atmosphere.

Because of the reduction in the incoming oceanic temperature, less heat is now going to be transferred from the ocean to the atmosphere so that the outgoing air will be cooler than before. Taking the incoming air temperature (T_{ai}) to be unaltered (because it is insulated from the ocean outside the box), we immediately find from (3) that the relationship between the reduction in temperature of the outgoing air and the reduction in the incoming oceanic temperature, is

$$\Delta T_{ao} = \frac{C_{\rho a}}{C_{\rho w}} \Delta T_{wi}. \tag{4}$$

This implies that the *maximum* ratio of the reduction in the temperature of the incoming ocean water and the temperature of the outgoing air is the ratio of the heat capacities which is about 1:4. [Note that the heat capacity of water is approximately 4.19 kJ/kg °C whereas the heat capacities of dry air and water vapor are 1.06 and 1.84 kJ/kg °C (respectively). Since the moisture content of air is no more than a few percent (kg per kg), it follows that the heat capacities ratio is about four]. In most situations, the actual ratio will be *less* than the above 1:4 upper bound because, as stated, there will be some alteration of the outgoing water temperature so that only a fraction of the oceanic heat anomaly will be transferred to the air.

Consistent with this upper bound, the Greenland air/water temperature anomaly ratio is a bit smaller than 4.0 (it is 3.5). The more involved climate models mentioned earlier suggest a *low latitude* ratio that is still lower (1.5–2.0). Incorporating both ends of the estimates (i.e., a 1.5 ratio and a 4.0 ratio), the atmospheric temperature reductions for events 1 through 5 will be taken to be roughly 3–8 °C, and 8–20 °C with the smaller estimates (1.5 ratio) corresponding to the more conservative choice based on the climate models (which involve evaporation, humidity and many other variables). We shall see later that a springs ice cover can occur even within the framework of the most conservative estimates.

The dense plume

This section is divided into two parts. First, we shall discuss the salinity and temperature of the springs during the cold events and then we shall discuss the resulting plume dynamics, i.e., its scales and structure.

Springs salinity and temperature

For simplicity, we take all the closely packed Tabgha springs (Figure 1) to be represented by a single source of salty and warm water. For reasons that were briefly mentioned earlier and will be elaborated on shortly, we shall consider the behavior of the plume during periods of *calm* winds.

Recent measurements of both the water properties and the local winds were taken by the Mekorot Water Corporation, a semi-private corporation that maintains the conduit diverting the springs. There is a seasonal variability in the salinity, temperature, and mass flux (e.g., Rimmer et al. 1999), but, for our purpose, it is sufficient to consider the mean values which correspond approximately to 3.7 PSU, 26 °C, and 0.7 m^3/s. (Note that documents describing the limnology of Lake Kinneret typically give the salt content in terms of chlorinity, which has a ratio of 1.7–2.1 to the total salt content.)

The springs water consists of a mixture of two distinctly separate ground water sources. The first is a deep, relatively steady source providing water with a salinity similar to that of the Mediterranean Sea, about 36 PSU (Rimmer et. al. 1999), and a high temperature of perhaps 63 °C which is the temperature of the (unmixed) Tiberias hot springs. The second is a more variable fresh water source resulting from rainwater percolating down to the aquifer. The Tiberias Springs, situated several kilometers to the south of the Tabgha, contain only the first source (i.e., no fresh water intrusion) and, hence, they are much saltier and much warmer than the Tabgha springs. Conservation of salt [i.e., $Q_1S_1 + Q_2S_2 = QS$, where Q_1, Q_2 and S_1, S_2 are the volume fluxes and salinities of the two incoming sources (so that $S_2 = 0$) and Q and S are the volume flux and salinity of the resulting spring mixture] immediately shows that the deep source (Q_1, S_1) provides about 10% of the mixed water

and that the remaining 90% comes from rain. (Note that the equivalent equation for conservation of heat cannot be used because the sources of underground heat cannot be easily estimated.)

We shall now estimate the corresponding values (S and T) during the five cold events that took place during the last 13,000 years. For simplicity, we assume that, due to the increased aridity, the rainfall was reduced by, say, 60% during the cold periods (Figure 2, lower panel). Since the present spring water is a 1: 9 mixture of deep and rain water, this 60% reduction in rain water implies that, during the cold periods (when the above ratio is modified to 1:3.6), only 78% of the mixture was from rain and the remaining 22% came from the deep water source (with a 37 PSU). This means that the adjusted springs' salinity that we should consider is 8.14 PSU. (Note that, because the springs' salt source is either the Mediterranean or previously percolated water, the increased evaporation during the cold, more arid, periods has almost no bearing on it.)

Since both the air and the rain were at least 3 °C cooler during the cold events than they are today and, since most of the springs' water is rain, we take the cold period springs water temperature to also be 3 °C cooler than the present springs water temperature of 26 °C (i.e., we take it to be 23 °C). Note, however, that, even with different choices for the rain reduction, our final results would essentially be the same—they are not very sensitive to these choices. Also, note that we shall not adjust the mass flux Q to the increased aridity because, as we shall shortly see, this has an effect only on the plume size, and this effect is very minor.

Our choices for the plume (T = 23 °C and S = 8.14 PSU) and winter lake variables (T = 15 °C and S = 0.5 PSU) are shown on the TS diagram Figure 4) which also displays the change of lake water density due to cooling leading to freezing (vertical dashed line). Figure 4 also shows the salinity and temperature of the water above the springs-induced plume both before and during freezing (dashed-dotted lines). These were computed using a (steady) solution to the vertical diffusion equation (discussed later) which gives a linear distribution. Note that cooling all the way down to freezing does not, at any point, involve convection because the springs-induced stratification always corresponds to water heavier than the cooled water above. This can be vividly seen by noting that, as the surface water is cooled (thick dashed vertical line), a density greater than the water below (dashed-dotted lines) is never reached.

Plume dynamics

Scales

The dynamics of heavy plumes have been studied extensively and the interested reader is referred to the first study by Smith (1975) and the more recent studies of Shapiro and Hill (1997), Killworth (2001) and the references given therein. Since we are merely interested here in the plume's scales, there is really no need to present any detailed solution. It is sufficient to show the main balances. Note that none of the dynamics and balances presented below is new – all the relationships that we shall employ can be found in one form or another in the earlier articles mentioned above.

When the wind stress is relatively weak, the general circulation in small lakes such as Lake Kinneret is usually cyclonic (e.g., Csanady 1982) because this is the direction in which both Kelvin and topographic Rossby waves propagate (see also Serruya 1974). This circulation forces the plume to deflect to the right (looking off-shore). This deflection is consistent with the condition that, because the offshore slope is large (1:100), the plume cannot descend offshore 'head-on' as it would become unstable if it were to do so. Instead, the plume picks its own bottom slope along which it can gradually progress without becoming unstable (Figure 5). We shall see that this picked path is in between the zero along-isobaths slope and the 1:100 cross-isobaths slope. It is much closer to the isobaths than it is to the offshore direction.

We can estimate the plume's speed, thickness, and width as well as the slope that it will follow, by considering the following balances. First, it is expected that frictional losses along the bottom of the plume will be compensated for by a pressure drop associated with the gradual decline in the mean plume height, i.e.,

$$g'\mu \sim CDu^2/\hat{H}, \tag{5}$$

where g' is the known 'reduced gravity', $(g\Delta\rho/\rho)$, μ the yet unknown slope along which the plume

progresses (as we said, not at all equal to the large cross-isobaths slope of 1:100), C_D a known non-dimensional drag coefficient for water over a solid surface (approximately 2×10^{-3}), u the unknown mean speed and $\hat{H}$ the unknown thickness of the plume. Second, the flow is required to be stable so that the Froude number is approximately unity implying,

$$u^2 \lesssim g' \hat{H}. \tag{6}$$

This condition (6), together with the energy constraint above (5), immediately shows that $\mu \sim C_D \sim 2 \times 10^{-3}$, implying that the plume veers slightly to the left of the isobaths (looking downstream) at an angle δ of approximately 18° (because the offshore slope μ_0 is 1:100 and the long-shore slope is zero). The third condition is the conservation of volume,

$$Q \sim u\hat{H}L, \tag{7}$$

where Q is the (known) constant volume flux and L is the unknown plume width. The fourth and last condition is a geometrical constraint (involving a cross-section of the plume) implying that,

$$\hat{H} \sim \mu_0 L \tag{8}$$

This condition states that, in order to have a thickness ranging from zero to $\hat{H}$, the plume's outer edge must be at least a distance L away

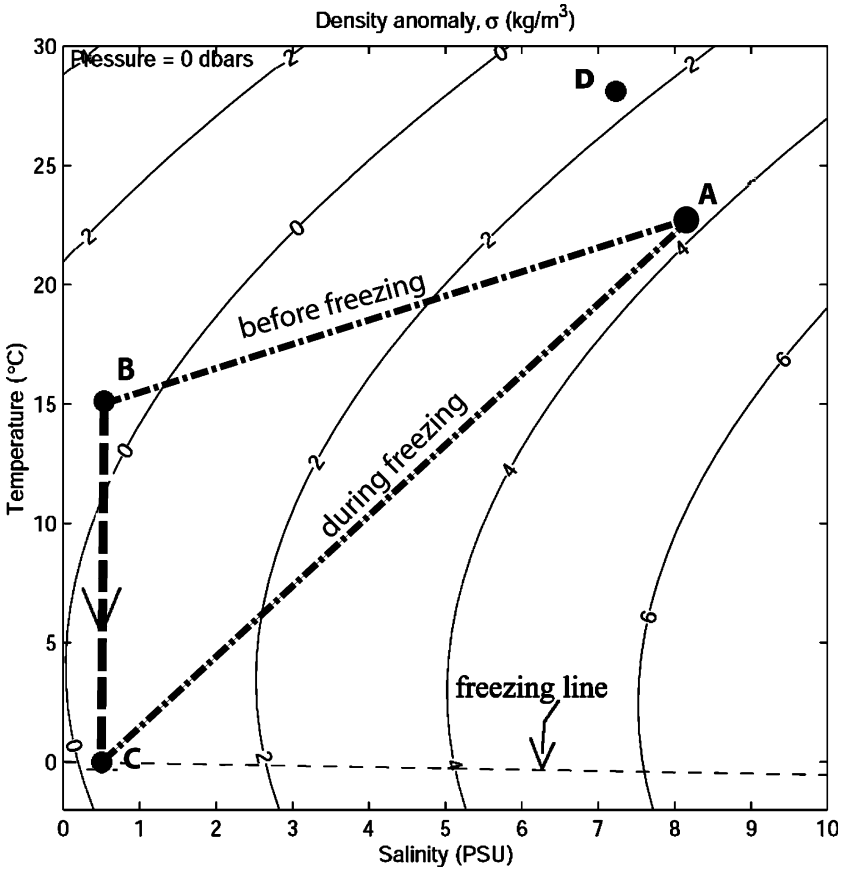

Figure 4. The mean density (during the cold events) of the springs water (A) and of the present-day lake water in winter (B). The salinity for the cold periods was adjusted to reflect the increased aridity. For a comparison, we also show the highest unadjusted variables of the most dense Tabgha spring, the Sartan Spring (D). The dashed-dotted lines represent the water above the springs before and during the freezing process. They are based on a linear solution to the diffusion equation (for heat and salt) and on the plausible assumption that the surface water above the springs has the same salinity as the off-shore lake water. Note that, as shown with the vertical dashed line (BC), cooling of the lake water above the springs causes freezing (C) without convection because the density associated with the cooling is always smaller than that of the water below.

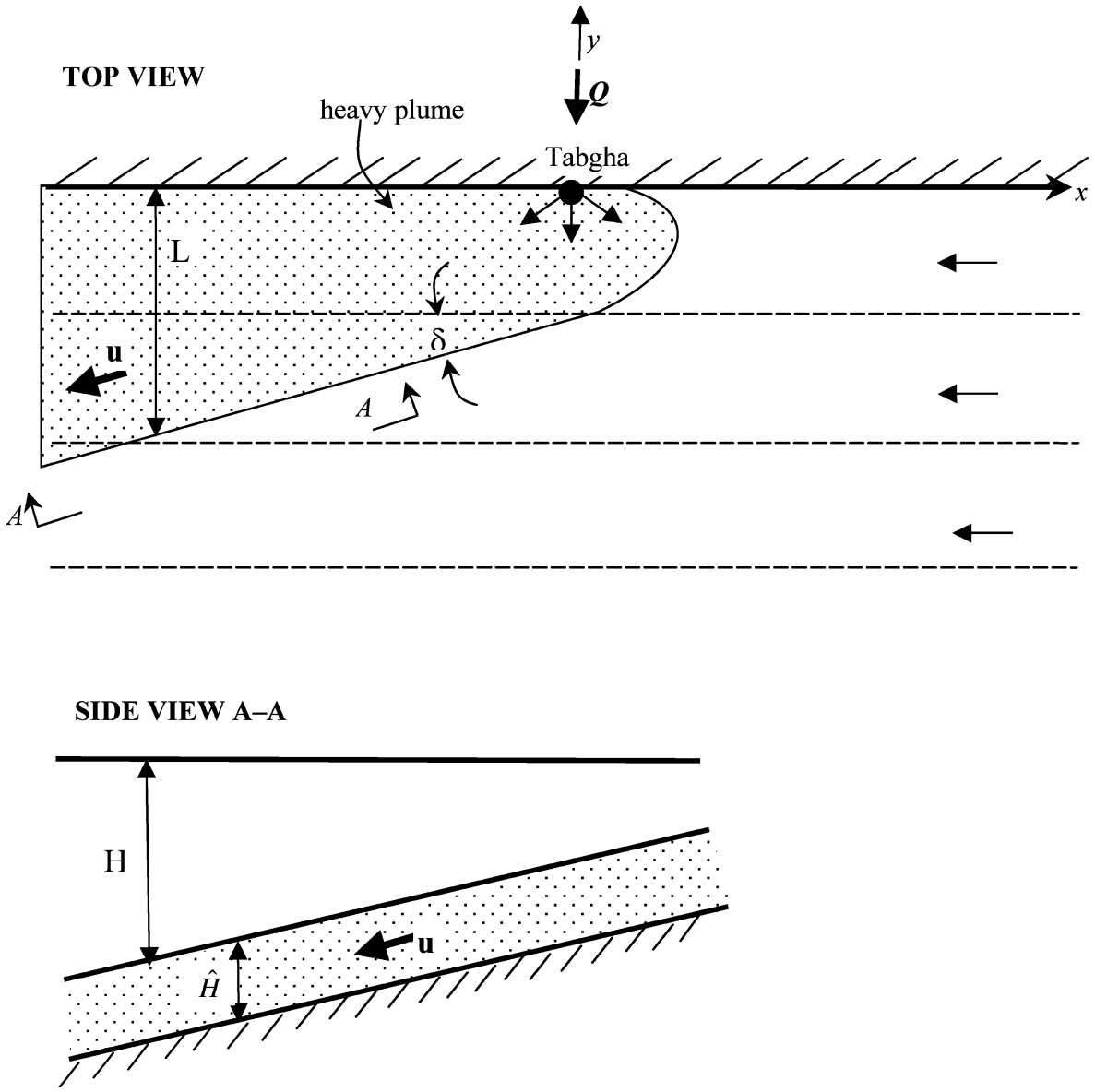

Figure 5. Schematic diagram of the plume's spreading along the bottom of the lake. Dashed lines represent the isobaths whose cross slope μ_0 is about 1:100. The general cyclonic circulation of the lake forces the plume to the right (looking off-shore) and the tendency of the plume to gradually lose height forces the plume to veer slightly to the left of the isobaths (looking downstream). The veering angle δ is approximately 18 °. This gradual veering is because the offshore slope μ_0 is so large that a 'head-on' descent would make the plume unstable. The slope that it follows is μ.

from the inner edge (where its thickness is zero). The four algebraic Eqs. (5–8) provide a solution for the four unknowns μ, u,$\hat{H}$, and L. We already obtained μ as 2×10^{-3} and a combination of (2), (3), and (8) gives,

$$\hat{H} \sim \left(Q^2 \mu_0^2 / g'\right)^{1/5}. \tag{9}$$

Taking Q to be $0.7\ \mathrm{m^3\ s^{-1}}$ and g' to be approximately $3 \times 10^{-2}\ \mathrm{ms^{-2}}$ (Figure 4), we find $L \sim 30$ m, $\hat{H} \sim 30$ cm and $u \sim 8\ \mathrm{cms^{-1}}$.

The plume is expected to be present in a region of O(1) meter deep. We shall see later that whether it is 1, 3, or 4 m deep makes no difference to our final conclusions.

The no-mixing condition

The approximately 30 cm-thick plume which is embedded in a meter or so of lake water can, of course, be mixed (with the fluid above) if the wind is strong enough. The condition of no convection requires that such mixing will not take place during the freezing period (of a few days). Hence, we require that the stress imposed by the wind will be so small that it will not be able to elevate the heavier plume and mix it with the lighter fluid above. In analogy with a wind set-up situation (where the wind elevates the water surface on the downstream side), we replace the free surface wind set-up elevation with the interface displacement times the ratio of the density difference to the density. Taking into account the plume length scale and the strength of the wind, we find that this mixing condition is,

$$g'H\hat{H} \sim \frac{\rho_a C_D U^2 L}{\rho_w}, \qquad (10)$$

where ρ_a and ρ_w are (as before) the air and water densities and U is the wind speed. Relation (10) can also be interpreted in terms of energy – the right hand side represents the work done (on the water) by the wind and the left represents the increase in potential energy (due to the lifting of the heavy fluid). For our earlier parameter choices, an air-on-water drag coefficient of 1/1000 and an H of 1 or 2 m, this relationship shows that $U \sim 15$ ms^{-1} is the necessary condition for mixing. This speed is relatively high because the plume is small and the stratification is relatively high.

For the region in question, this speed is so high that it has never been observed even once in the entire 5 years hourly record that we looked at. (The highest speed that was recorded was less than 12 m/s.) To avoid this mixing situation, we require that the wind be less than 6 m/s (less than a half of the mixing speed) for the entire freezing period. This is certainly an adequate choice as the wind stress is proportional to the square of the wind speed so that a quantity less than a half will produce little mixing.

We shall see later that, in winter, the wind speed exceeds this value only during strong storms. For all practical purposes, the above restriction on the wind corresponds to an almost no-wind state. Hence, it corresponds to a lake with very small eddy diffusivity, close to the molecular diffusivity. In this context, it is of interest to note that measurements conducted in ice-covered lakes (which have no wind input but do have convection due to heat released from the sediments on the bottom) reveal a horizontal eddy diffusivity of 100 cm^2/s (Bengtsson 1996). Together with the length-to-depth ratio of 100:1 in the lake, this gives vertical eddy diffusivity identical to the molecular diffusivity, 0.01 cm^2/s. This is consistent with the idea that, although the plume itself is turbulent, the turbulence is expected to die off at a distance of the order of the plume thickness (30 cm) away from it.

The above decay of mixing is expected to take place within a few minutes after the winds die down (because this is the time that it takes heavy particles to sink and buoyant particles to rise). As we shall see, a linear profile of both temperature and salinity will be established above the plume. It is not easy to say how long it would take for such a profile to be established but, if it were to start from a state of rest, then molecular diffusion would set it up within a few or several days. On the other hand, if it were to start from a completely mixed state then it would be achieved within a few minutes after the winds die down.

The ice model

Fresh and brackish water follow a complicated freezing process which involves convection and complete turnover. This is because the maximum density of fresh and brackish water is around 4 °C implying that, before a fresh water lake can freeze on top, all of its water must first be cooled to 4 °C. When this stage is reached and the cooling continues to temperatures below 4 °C, the newly cooled water is lighter than the warmer water underneath so that it floats and stays on top until the freezing condition of 0 °C is reached. On the other hand, sea water ($S > 24$ PSU) which is typically *weakly* stratified by the salt (i.e., the density gradient due to salt is not much greater than that induced by temperature) does not have such a maximum. As a result, newly cooled surface sea water with a temperature below 4 °C is no longer lighter than the water below so it does not stay on top. Consequently, some

convection (limited to the upper portion of the water column) occurs before freezing. Namely, the freezing of fresh water involves a complete convection and turnover whereas the freezing of sea water normally involves a partial convection. (Note the two do not occur at the same temperature.)

A body of water which is *strongly* stratified by salt (i.e., the salt gradient overwhelms the density gradient) behaves in a way which is different from the previous two. Here, there is no convection at all. This is because the cooling of surface water cannot overcome the stabilizing effect of the salt. If one compares a hypothetical strongly stratified salty lake (i.e., a salty lake with salt-induced density anomaly greater than that induced by the temperature gradients) and a fresh water lake of the same size both having an initial temperature of, say, 15 °C, then much more cooling is required to form ice on top of the fresh water lake than on top of the strongly stratified salt lake.

This is because the entire fresh water lake must first be cooled to 4 °C whereas the salt-stratified lake can freeze on top even if most of its water stays at 15 °C. We argue that the situation above the Kinneret springs' plume corresponds to such a strongly stratified salty lake. This is clearly reflected in the $T-S$ diagram shown in Figure 4. The straight, dashed-dotted lines show the density of the water above the springs' plume just before cooling starts and during the freezing process. These lines were constructed using the linear solution to the (steady) diffusion equation, and off-springs lake water salinity at the surface. Note that at no point during the cooling process (thick dashed vertical line) is the surface water heavier than the water below.

Ice modeling background

The first ice growth model was developed by Stefan (1890), who correctly identified the most important freezing processes – the atmosphere cools the ice from above and the conversion of water into ice occurs along the ice-water interface (without significant exchange of heat from below). Stefan took the transfer of heat within the ice to be linear and this leads to a linear first-order differential equation which has a straightforward solution. A good summary of Stefan's work, as well as of straightforward extensions of his work, is given in Neuman and Pierson (1966). The next step was made by Welander (1977), who, in effect, broadened Stefan's work. Welander considered a laboratory situation where the ice exchanged heat with the fluid below (which receives a constant amount of heat from a laboratory heater) and the air above. The temperature of the fluid below the ice changes with time and the model equations are nonlinear. Welander obtained a numerical solution to the problem. For more recent and more involved numerical ice simulations, the reader is referred to Kantha and Mellor (1989), Mellor and Kantha (1989) and Hakkinen (1995). Although these recent numerical models as well as Welander's model are of interest, they are much more involved and complicated than what we need here. Since we are merely interested in a reasonable estimate, an analytical one-dimensional model is sufficient.

Our adopted model differs from both Stefan's (1890) and Welander's (1977) models. Stefan's model does not include heat exchange from below which is important in our case because the salty springs are warm. Welander's model, though it included heat transport from below, allowed the temperature below to change with time. Because the spring water temperature does not vary much over the time scale that the ice is formed (days) and because the ice thickness (on the order of 10 cm) is much smaller than that of the relatively fresh water above the spring water (on the order of 1 m), our heat exchange with the fluid below can be taken to be constant. We shall see that, even though this heat flux is constant, it still alters Stefan's equation dramatically. It turns out, however, that a simple transformation allows one to obtain an exact analytical solution. This was recognized earlier by Thorndike (1992) who considered a somewhat different physical system than ours but ended up with the same equation that we have here. Leppaeranta (1993) argues that, if one takes the air temperature to be equal to the ice surface temperature, then the Stephan's model overestimates the ice thickness. This overestimate is supposedly particularly important for thin ice such as ours. However, it is based on Anderson's (1961) analysis for sea-ice which is normally

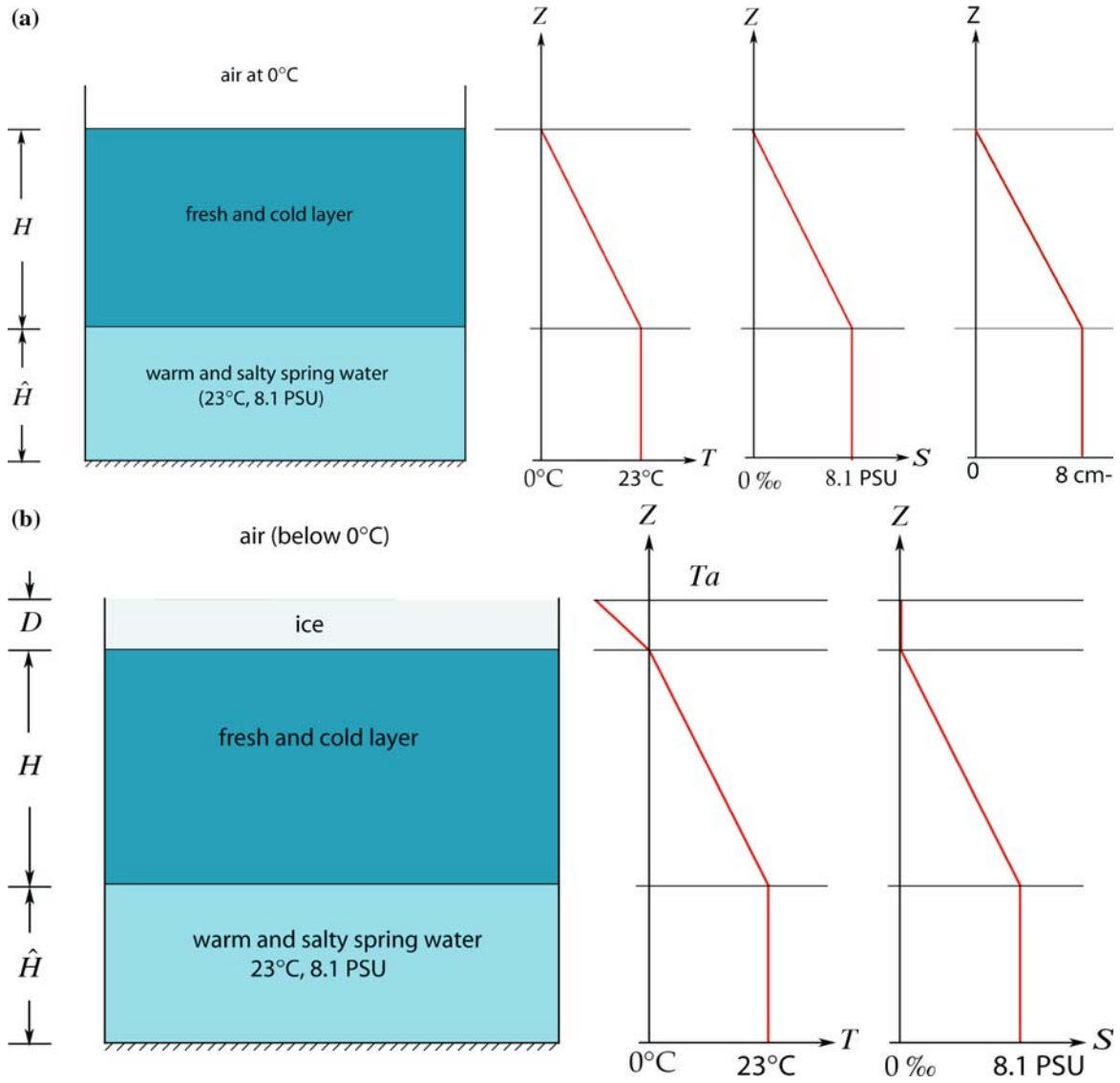

Figure 6. (a) Schematics of the initial conditions immediately prior to the initiation of ice. This situation is established within a day or so after the winds die down, so that there is very little vertical mixing. Along the bottom, there is a layer ($\hat{H}\sim30$ cm) of warm and salty spring water. The layer on top ($\hat{H}\sim1$ m) is lake water (0.5 PSU). For such a 'steady' situation, the diffusion equation immediately implies that both T and S, as well as the speed u, are linearly distributed in the upper layer. The surface temperature is taken to be zero because this is what the atmosphere imposes. Similarly, the surface salinity is taken to be almost zero because these waters are off-shore lake water. The velocity is taken to be zero at the surface because of friction along the ice–water interface. (b) The conditions during ice formation. The ice thickness, D (on the order of $\sim$10 cm) is taken to be much smaller than H (on the order of 1 m) so that, below the ice, the temperature and salinity profiles are taken to be the same as those with $D = 0$ (a). Note that there is no brine rejection, as the water that ultimately freezes is taken to be fresh water ($S = 0$).

subject to strong winds. It is not at all obvious how can the sea ice results be extended to inland lakes which are usually subject to weak winds. In view of this and the fact that we are merely interested in rough estimates, we shall not be concerned with this point.

Governing equations

Consider the situation shown in Figure 6a, b. Within the ice and within the light layer underneath the ice, the temperature is governed by,

$$\frac{\partial T_i}{\partial t} = a_i \frac{\partial^2 T_i}{\partial^2 z^2} \quad \text{(a)}$$
$$\frac{\partial T_w}{\partial t} = a_w \frac{\partial^2 T_w}{\partial^2 z^2}, \quad \text{(b)} \qquad (11)$$

where T_i and T_w are the temperatures of the ice and water, and a_i and a_w are the diffusivity coefficients ($a = k/\rho C_p$ where k is the thermal conductivity, C_p the specific heat and ρ, the density). An equation similar to (11a) controls the diffusion of salt above the plume. Assuming that the diffusion process is quasi-steady, the derivatives with respect to time are set to zero. This immediately shows that the temperatures are linearly distributed both within and underneath the ice. (The salinity is also linearly distributed above the plume.) In view of these, the heat flux within the ice (φ_i) is given by,

$$\varphi_i = k_i \frac{T_a}{D}, \qquad (12)$$

where T_a is the temperature of the air above the ice, D is the ice thickness, k_i is thermal conductivity through the ice, and the temperature of the ice at the ice-water interface was taken to be zero. Similarly, the heat flux in the layer immediately below the ice is

$$\varphi_w = k_w \frac{T_w}{H}, \qquad (13)$$

where H is the thickness of the layer above the spring water (1 or 2 m) and T_w is the temperature of the salty and heavy spring water below. Note that, for similar reasons, the velocity is also linearly distributed above the plume.

Along the ice–water boundary the heat-transfer equation can now be written as,

$$\rho_i \lambda_i \frac{dD}{dt} = -k_i \left(\frac{T_a}{D}\right) - k_w \left(\frac{T_w}{H}\right), \qquad (14)$$

where ρ_i is the ice density and λ_i is the ice heat of fusion. The term on the left represents the change of heat due to ice formation. The first term on the right is the heat flux through the ice (positive when ice is formed because $T_a < 0$). The second is the heat flux from below. When $T_w \to 0$ the problem reduces to the Stefan's (1890) problem. When T_w is not a constant but rather a function of time and height, the problem becomes Welander's (1977) oscillatory system. In our case, T_w is a constant of 26 °C. Note that the advection of heat by the horizontally moving water immediately below the ice has been ignored because the flow there is laminar and, just like the temperature and salinity, the speed vanishes along the ice–water interface.

Setting, for convenience,

$$\alpha = k_w T_w / H \rho_i \lambda_i, \quad \beta = k_i T_a / \rho_i \lambda_i \qquad (15)$$

Eq. (14) becomes

$$D \frac{dD}{dt} + \alpha D + \beta = 0, \qquad (16)$$

which is a nonlinear differential equation in D. Note that both terms defined by (15) are taken to be constants (i.e., they do not vary with time). We see that, even though the term that was added to Stefan's equation is linear [second term on the left side of (16)], it has changed the character of the equation from nonlinear homogeneous into a nonhomogeneous one. As recognized by Thorndike (1992), this difficulty can be overcome, however, by first re-writing (16) in the form,

$$dt = \frac{-D dD}{\alpha D + \beta}. \qquad (17)$$

Since the right-hand side is only a function of D and the left is only a function of t, we can simply integrate (17),

$$\int_t^0 dt = -\int_D^0 \frac{D dD}{\alpha D + \beta}, \qquad (18)$$

where we took $D = 0$ at $t = 0$ as the initial condition for ice formation. The solution is,

$$t = -D/\alpha + \frac{\beta}{\alpha^2} \ln\left(1 + \frac{\alpha D}{\beta}\right), \qquad (19)$$

which, for reasonable values of α, β, and D, is shown in Figure 7. Note that the second term in the brackets is negative for ice growth because β is negative ($T_a < 0$). This means that αD must be smaller than $|\beta|$. When $\alpha D > |\beta|$ then more heat is supplied to the ice from below than the heat removed from the top, and, consequently, the ice melts. Of course, (17) describes both melting and

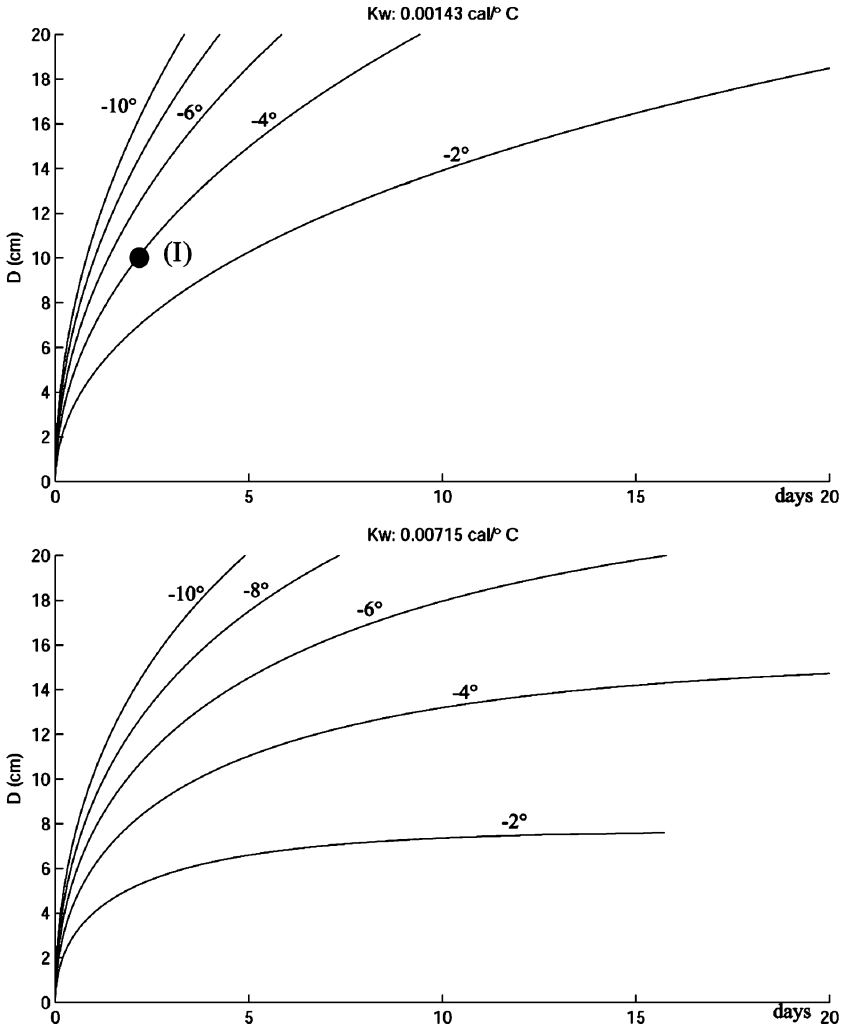

Figure 7. Predicted ice thickness (D) as a function of the air temperature and time according to (19). The upper panel shows the ice growth for a no-wind situation corresponding to a molecular diffusivity underneath the ice. Although this is the situation which we argue is relevant to Lake Kinneret, for completeness we also show the ice growth plot for an eddy diffusivity which is five times higher (lower panel). Point I corresponds to the cooling spell scenario which we, fairly arbitrarily, chose here. In making this choice we assumed that, in order to support a person, the ice thickness needs to be larger than 10 cm.

freezing, but the initial condition that we took in (18) corresponds *only* to freezing. (Melting requires that D will not be zero at $t = 0$.)

When the heat supplied from below is much smaller than the heat removed by the cold air above (i.e.,$\alpha D << |\beta|$), we can expand the second term in (19) to get,

$$t = -\frac{D^2}{2\beta}\left(1 + \frac{2\alpha D}{3\beta} + \frac{\alpha^2 2}{4\beta^2} + \cdots\right). \qquad (20)$$

For $\alpha \to 0$, (20) reduces to Stefan's relationship as should, of course, be the case. In the next section, we shall use the results of (19), as shown in Figure 7, to calculate the probability of a springs ice.

Before doing so, it is appropriate to point out that, regardless of the plume, the shallow regions of any high-latitude lake under moderate wind conditions always freeze over first. This is because the wind mixes the water down as far as 20 m thus retarding the freeze in the deep parts of the lake (see e.g., Omstedt 1998, 1999). This may appear at first to be relevant to our process but it really has no bearing on the problem at hand because it requires much more initial cooling than our

springs freeze does. As already alluded to, this familiar freezing process requires getting the entire lake down to 4 °C before freezing starts along the shore. (Our freeze does not require such a severe initial cooling.) As a result, the likelihood that such a shore line freeze occurred during the past 12,000 years is virtually zero. Furthermore, in these high-latitude lakes the cooling processes last weeks or even months so wind action is important whereas, in our case, the absence of wind for a few or several days is a common situation, particularly during a cold spell.

Recurrence times for springs ice

In this section we shall compute the likelihood of a cold spell strong enough to produce springs ice. We shall focus on the scenario shown in Figure 7. The 17-year time series data plotted in Figure 8 are mean daily air temperatures at Tabgha for October 1986–December 2003 (as obtained from Mekorot, Israel Water Company). Our approach is to fit a seasonal time series model to these data, then to simulate output from the fitted model under various cooling events. Note that a 'cooling event' is very different from what we refer to as a 'cooling spell.' A 'cooling event' corresponds to paleoclimatological cooling over a period of order of 100 years or more (Figure 2), whereas a 'cooling spell' is a brief (on the order of few days) period of below-freezing temperatures. The two are distinctly different and it is important to keep the distinction in mind as we shall focus on situations where both occur at the same time.

Simulated output from the statistical fitted model, over a 100,000-year time period, is used to estimate the expected number of years between two freezing events (the recurrence time). We consider a situation where the average air temperature drops below −4 °C for two days. This choice is made on the basis of the calculations shown in Figure 7 and corresponds to the solid dot shown there (top panel).

First, we decomposed the time series data into seasonal and residual components using the S-PLUS function stl (Venables and Ripley, 2002, Section 14.3). The seasonal pattern was found to be unstable over the last 8 years, but fairly stable before that. Thus, only the first 9 years of data were deemed suitable for use in the subsequent model fitting. The residual, after removal of the seasonal component, was then modeled as a lag-3 autoregressive process, i.e., AR(3). After removal of both the seasonal and AR(3) components, the residual plots displayed some wild transitory behavior (as often seen, for example, in financial time series data), so we used the S+GARCH module to add a GARCH (1,1) component with normal conditional distributions to further refine the model (see Venables and Ripley, 2002, Section 14.6, for further discussion and references on this

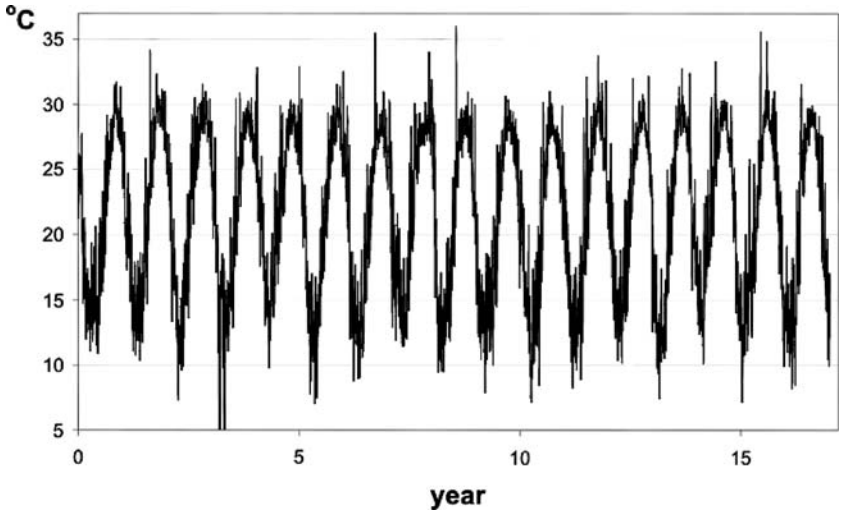

Figure 8. Tabgha daily mean air temperature (°C) vs. years, from October 1, 1986 through December 2003.

type of statistical time series modeling). Note that after removal of the seasonal component and the overall mean, the fitted AR(3) model is,

$$X_t = 0.905X_{t-1} - 0.299X_{t-2} + 0.136X_{t-3} + R_3.$$

The fitted GARCH (1,1) model for the residual *Rt* is,

$$R_t = 0.042 + \eta_t, \quad \eta_t = \sigma_t \varepsilon_t,$$
$$(\sigma_t)^2 = 0.037 + 0.116(\eta_{t-1})^2 + 0.876(\sigma_{t-1})^2,$$

where the ε_t are independent $N(0,1)$ random variables.

Our simulation results for the final fitted time series model give the expected recurrence times for springs ice under mean air temperature cooling in the range of 2–20 °C. As mentioned, these cold *events* need to be distinguished from the cold *spells* that would cause a temporary freeze, because the cold events represent the mean cooling which took place over many years (as shown in Figure 2). We find that a mean 3 °C atmospheric cooling (i.e., events 1, 2 and 3 subject to our *lower* air/water temperature ratio of 1.5) is likely to produce (on average) springs ice every 119 years. For the high (upper bound) ratio of air/water temperature anomaly (4), the atmospheric temperature anomaly is fairly large (8 °C) and the corresponding recurrence time is short, once in 14 years. Similarly, for a mean cooling of 7 °C (event 4 and 5 subject to our lower ratio of 1.5), the recurrence time is 20 years. A 20 °C air temperature reduction (i.e., our high water/air temperature ratio of 1:4 applied to events 4 and 5) corresponds to a continuous production of springs ice during the entire winter. (A rough heat budget calculation shows that, with a 20 °C cooling event, freezing covering the entire lake might have also been possible but our model does not apply to such convection and freezing process so we cannot say much about it.)

To arrive at our final recurrence time, we now need to incorporate the no-mixing condition implying that the cooling spells take place at times with no winds of more than 6 m/s. To calculate this, we took the winter (1st of November to the 1st of March) hourly wind intensity data from 5 years (January 1999–December 2003) and looked at the number of times that a period of consecutive 48 h elapsed without the wind intensity exceeding 6 m/s even once. This gives 73% as the probability that the intensity of the winds will *not* exceed 6 m/s in a 2 days period. Using the same data set, we then looked at the correlation between times of strong winds and periods of strong cooling. Like many other parts of the northern hemisphere (e.g., the USA), typical winter cooling is associated with a low pressure system passing over the region. First, the region experiences the outer parts of the low which involves strong winds and then, after a few days during which the winds died down, it experiences the coldest temperatures. This phase lag suggests that our freezing period will *not* be associated with strong winds.

In view of these, we get that the recurrence time for a freeze during events 1 and 2 and 3 is once every 163 years (i.e., 119/0.73) for the smallest (conservative) choice of the air temperature anomaly (3 °C) and once in 19 years for the largest (least conservative) choice (8 °C). During events 4 and 5 the recurrence time is once in 27 years for the smallest (conservative) choice of atmospheric anomaly (7 °C). For the largest (the least conservative choice of 20 °C), there were continuous springs ice forming during the entire winter. It is difficult to tell from Figure 2 just how long cooling events 1, 2, and 3 were. However, since 100 years is within the resolution of that figure, it is fair to assume that the length of these events is on the order of 100 years, implying a large likelihood of springs ice occurring during events 1, 2 and 3. This is also the case for events 4 and 5.

Summary

We have presented two separate lines of investigation. The first is a rigorous theoretical and analytical investigation of the likelihood of ice formation above the salty springs. The second is a less rigorous examination of the idea that such a freeze was the origin of the walking on water story.

With the idea that much of our cultural heritage is based on human observations of nature, we sought a natural process that could perhaps explain the origin of the account that Jesus Christ walked on water. Our general approach is similar to that we adopted earlier to explain the parting of the Red Sea where we proposed that a strong wind action caused a wind set-down which exposed a usually submerged ridge (Nof and Paldor 1992). It

is also similar to Ryan and Pitman (1998), who attempted to explain the biblical flood arguing that it originated in the abrupt initiation of strong flows into the (then fresh water lake) Black Sea at the very end of the last glaciation (about 6000 years ago). These strong flows came about when, due to the melting of ice sheets, the sea level rose above the sill depth in the Bosphoros (Ryan et al. 2003). Neither one of these theories provide an exact explanation of the biblical stories – our own Red Sea parting theory does not fit the biblical story in terms of the wind direction, and Ryan and Pitman's explanation does not fit in terms of its limited nonglobal extent. Similarly, our present explanation does not exactly address 'walking on water' but rather provides a plausible physical process that has some characteristics similar to those described in the New Testament. Despite these differences, and mismatches, we believe that all of those explanations add to our understanding of our own and our ancestors' lives.

Recognizing that a significant part of Christ's life was spent in Tabgha next to Lake Kinneret, the thought that limited parts of the lake froze during some past cooling spells came to mind. Initial calculations showed that, due to convection, which is a common pre-freezing condition in freshwater lakes, a total freeze of the entire lake or even isolated parts next to the shore was not possible because there was not sufficient cooling to bring the lake down to 4 °C. Noting that the dense (warm and salty) Tabgha springs (Figure 1), which until the 1960s emptied into the lake, can provide a localized shield from convection, we focused on the dynamics of the region next to the springs.

Since the springs water is heavier than the lake water, they set up a stratified region above their associated plumes (Figure 6a). As the $T-S$ diagram (Figure 4) shows, this stratification is a barrier to convection (see also Figure 6b). In these regions above the plumes, freezing during events 1, 2 and 3 appears to be possible because only the top water had to be cooled down to the freezing point, i.e., the entire lake stayed much warmer than 4 °C. Using the nonlinear one-dimensional ice-water equations, we derive a solution to the ice growth problem [Figure 7 and (19)]. It shows, for example, that, although the top is warmed from below by the spring water, atmospheric cooling down to −4 °C for merely 2 days is sufficient to produce an

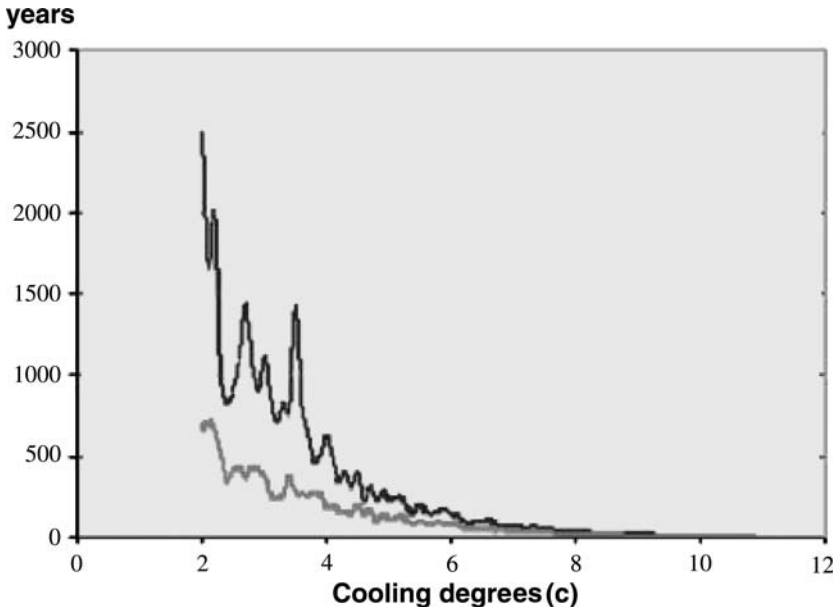

Figure 9. Typical recurrence time of springs ice in Lake Kinneret as a function of mean air temperature cooling. Note that these are cooling spells and not cooling events. The wild fluctuations in the plot represent Monte Carlo error which decreases with cooling. The upper line represents the case where the lake (above the plume) is cooled to −2 °C for 9 days whereas the lower represents the case where the lake is cooled to −4 °C for 4 days. These are hypothetical cases and are shown here merely for clarity. The value that we actually chose for our detailed calculation (−4 °C cooling for 2 days) is discussed at length in the text and is not shown here.

ice cap which is 10 cm thick, i.e., thick enough to support human weight.

It is, of course, desirable to extend these results of our analytical (nonlinear) one-dimensional model to three dimensions (particularly to examine the question of whether a significant amount of new lake water can be advected from the sides into the region above the plume while the freezing is taking place). This can be done numerically but is left as a subject for future investigation because previous three-dimensional high-resolution numerical studies of ice formation have shown that the difference between their predictions and those of the analytical one-dimensional models is fairly limited (e.g., Omstedt, 1999).

We also performed a statistical analysis based on both air temperature records and wind records, and concluded that the above cooling spells had a recurrence time of once every 163 years during the first (1500 years ago), second (2500 years ago) and third (9800 years ago) cooling events (Figures 2, 8 and 9). Since these cooling events appeared to have lasted longer than our most conservative estimate of a 163-year period, we concluded that the likelihood of a springs ice occurring during the last two cooling events is substantial. During the Younger Dryas, springs ice formation was more common.

Because the size of the springs ice (which can, by the way, be partially anchored to the shoreline) is relatively small (30 m), a person standing or walking on it would appear to a distant observer to be 'walking on water.' This is especially true for those who were not used to see ice on the lake, particularly if it rained after the ice was formed. In a way, this is similar to what is frequently observed today in high latitude lakes – when it rains, the ice surface becomes so smooth that it appears to a distant observer as if skaters are 'skating on water'.

We hesitate to draw any conclusion regarding the implications of this study to the actual events that took place at Tabgha during the last few (or several) thousand years. Our springs ice calculation may or may not be related to the origin of the account of Christ walking on water. The whole story may have originated in local ancient folklore which happened to be told best in the Christian Bible. It is hoped, however, that archeologists, religion scholars, anthropologists and believers will examine such implications in detail.

Acknowledgements

This work could not have been completed without the help of many individuals. Steve VanGorder helped with the calculations leading to Figure 7 and critically read the manuscript more than once. Through Benjamin TalTesch, Mekorot, Israel Water Company, provided us with both the air temperature record and the wind record, as well as information regarding the temperature, salinity, and mass flux of the springs. Communications with Matthew Huber, Alon Rimmer, Ayal Anis, Lakshmi Kantha, Kevin Speer, David Lea, Jeff Chanton, Georges Weatherly, Lou St. Laurent, John A. Young and Dale Haidvogel were all very helpful. (Note, however, that they never really knew exactly what we were working on so their communications with us do not necessarily reflect their support of our views.) Important comments on an earlier draft were made by Hezi Gildor; Barbara French provided comments on the social aspects of the work. Although none of our grants were specifically awarded with the purpose of supporting this particular study, our recent research has been supported by the National Science Foundation Grants OCE- 9911324 and OCE-0241036, the National Aeronautics and Space Administration Grants NAG5-7630 and NGT5-30164, and the Binational Science Foundation grant BSF 96-105. Both Florida State University (through the Oceanography Department, the Geophysical Fluid Dynamics Institute and the Statistics Department), and the Hebrew University (HU) provided support through our regular faculty appointments, and the Ring Foundation at the HU supported DN's recent visit to Jerusalem in 2003.

References

Anderson D.L. 1961. Growth rate of sea ice. J. Glaciol. 3: 1170–1172.

Antenucci J.P. and Imberger J. 2003. The seasonal wind/internal wave resonance in Lake Kinneret. Limnol. Oceanogr. 48: 2055–2061, ED 1276.

Bard E. 2002. Climate shock: abrupt changes over millennial time scales. Phys. Today 55: 32–38.

Bar-Matthews M., Ayalon A., Gilmour M., Matthews A. and Hawkesworth C.J. 2003. Sea–land oxygen isotopic relationships from planktonic foraminifera and speleotherms in the Eastern Mediterranean region and their implication for pa-

leorainfall during interglacial intervals. Geochim. Cosmochim. Acta 67: 3181–3199.
Bartov Y.S., Goldstein L., Stein M. and Enzel Y. 2003. Catastrophic arid episodes in the Eastern Mediterranean linked with the North Atlantic Heinrich events. Geology 31: 439–442.
Bengtsson L. 1996. Mixing in ice-covered lakes. Hydrobiologia 322: 91–97.
Bryson R.U. and Bryson R.A. 1998. Application of a global volcanicity time-series on high-resolution paleoclimatic modeling of the Eastern Mediterranean. In: Issar A.S. and Brown N. (eds), in Times of Climatic Change. Kluwer Academic Publishers, London, pp. 1–19.
Cacho I., Grimalt J.O., Canals M., Sbaffi L., Shackleton N.J. and Zahn R. 2001. Variability of the western Mediterranean Sea surface during the last 25000 years and its connection with the Northern Hemisphere climatic changes. Paleoceanography 16: 40–52.
Csanady G.T. 1982. Circulation in the Coastal Ocean. D. Reidel.
Cullen H.M., Kaplan A., Arkin P.A. and Demenocal P.B. 2002. Impact of the North Atlantic oscillation on Middle Eastern climate and streamflow. Climatic Change 55: 315–338.
De Rijk S., Hayes A. and Rohling E.J. 1997. Eastern Mediterranean sapropel SI interruption: an expression of the onset of climatic deterioration around 7 ka BP. Mar. Geol. 153: 337–343.
Dutton J.A. and Bryson R.A. 1962. Heat flux in Lake Mendota. Limnol. Oceanogr. 7: 80–97.
Emeis K.C., Struck U., Schulz H.M., Rosenberg R., Basconi S., Erlenkeuser H., Sakamoto T. and Martinez-Ruiz F. 2000. Temperature and salinity variations of Mediterranean Sea surface waters over the last 16000 years from records of planktonic stable oxygen isotopes and alkenone unsaturation ratios. Palaegeogr. Palaeocl. 158: 259–280.
Eshel G. and Farrell B.F. 2000. Mechanisms of Eastern Mediterranean rainfall variability. J. Atmos. Sci. 57: 3219–3232.
Guilderson T.P., Fairbanks R.G. and Rubenstone J.L. 1994. Tropical temperature variations since 20000 years ago: modulating interhemispheric climate changes. Science 263: 663–665.
Hakkinen S. 1995. Seasonal simulation of the southern ocean coupled ice-ocean system. J. Geophys. Res. 100: 22733–22748.
Hurwitz S., Stanislavsky E., Lyakhovsky V. and Gvirtzman H. 2000. Transient groundwater–lake interactions in a continental rift: Sea of Gaililee Israel. Geol. Soc. Am. Bull. 112: 1694–1702.
Kantha L. and Mellor G.L. 1989. A two-dimensional coupled ice-ocean model of the Bering Sea marginal ice zone. J. Geophys. Res. 9: 10921–10936.
Killworth P.D. 2001. On the rate of descent of overflows. J. Geophys. Res. 106: 22267–22275.
Lea D.W., Pak D.K., Peterson L.C. and Hughen K.A. 2003. Synchroneity of tropical and high-latitude Atlantic temperatures over the last glacial termination. Science 301: 1361–1364.
Lepparanta M. 1993. A review of analytical models of sea-ice growth. Atmos.–Ocean 31: 123–138.
Mellor G.L. and Kantha L. 1989. An ice-ocean coupled model. J. Geophys. Res. 9(C8): 10937–10954.
Nadel D., Weiss E., Simchoni O., Tsatskia A., Danin A. and Kislev M. 2004. Stone age hut in Israel yields worlds' oldest evidence of bedding. Proc. Natl Acad. Sci. 101: 6821–6826.
Neuman G. and Pierson W.J. 1966. Principles of Physical Oceanography. Prentice-Hall.
Nof D. and Paldor N. 1992. Are there oceanographic explanations for the Israelites' crossing of the Red-Sea??. Bull. Amer. Meteor. Soc. 73: 305–314.
Omstedt A. 1998. Freezing Estuaries and Semi-Enclosed Basins. Physics of Ice-Covered Seas. Helsinki University Press 2: 483–516.
Omstedt A. 1999. Forecasting ice on lakes estuaries and shelf seas. Ice Phys. Nat. Environ. 1: 185–207.
Pinot S., Ramstein G., Harrision S.P., Prentice I.C., Guiot J., Stute M. and Joussame S. 1999. Tropical paleoclimates at the last glacial maximum: comparison of paleoclimate modeling intercomparison project (PMIP) simulations and paleodata, Clim. Dyn. 15: 857–874.
Pixner B. 1985. The miracle church of Tabgha on the Sea of Galilee. Biblical Archaeol. 46: 196–206.
Reale O. and Dirmeye P. 2000. Modeling the effects of vegetation on Mediterranean climate during the Roman Classical Period Part I: climate history and model sensitivity. Global Planet. Change 25: 163–184.
Rimmer A., Hurwitz S. and Gvirtzman H. 1999. Spatial and temporal characteristics of saline springs: Sea of Galilee Israel. GroundWater 37: 663–673.
Ryan W.B.F., Major C.O., Lericolais G. and Goldstein S.L. 2003. Catastrophic flooding of the Black Sea. Annu. Rev. Earth Planet. Sci. 31: 525–554.
Ryan W. and Pitman W. 1998. Noah's Flood: The New Scientific Discoveries about the Event that Changed History. Simon & Schuster, New York.
Serruya S. 1974. The mixing patterns of the Jordan River in Lake Kinneret. Limnol. Oceanogr. 19: 175–181.
Shapiro G.I. and Hill A.E. 1997. Dynamics of dense water cascades at the shelf edge. J. Phys. Oceanogr. 27: 2381–2394.
Shin S.I., Liu Z., Otto-Bliesner B., Brady E., Kutzbach J. and Harrison S. 2003. A simulation of the last glacial maximum climate using the NCAR-CCSM. Clim. Dyn. 20: 127–151.
Stefan J. 1890. Über die Theorie der Eisbildung in Spesondere über Eisbilding im Polarmeer Stiz. Ber. Kais. Akad. Wiss. Wein 98(2A): 965.
Stute M., Forster M., Frischkorn H., Serejo A., Clarke J.F., Schlosser P., Broecker W.S. and Bonani G. 1995. Cooling of Tropical Brazil (5°C) during the last glacial period. Science 269: 379–383.
Thorndike A.S. 1992. A toy model linking atmospheric thermal-radiation and sea ice growth. J. Geophys. Res. 97(C6): 9401–9410.
Venables W.N. and Ripley B.D. 2002. Modern Applied Statistics with S (4th ed.). Springer.
Welander P. 1977. Thermal Oscillations in a fluid heated from below and cooled to freezing from above. Dyn. Atmos. Ocean. 1: 215–223.